Journal of
Materials Chemistry B

Materials for biology and medicine

Accepted Manuscript

This article can be cited before page numbers have been issued, to do this please use: B. Paila, S. Asok and A. K. Suresh, *J. Mater. Chem. B*, 2026, DOI: 10.1039/D5TB02620B.

ROYAL SOCIETY OF CHEMISTRY

rsc.li/materials-b

Physicochemical Stability and Protein Corona Profiling on the Interaction of Iron Oxide Nanoparticles with Human Tear

Bhagyasree Paila, Sneha Asok and Anil K. Suresh*

Bionanotechnology and Sustainable Laboratory, Department of Biological Sciences, School of Engineering and Applied Sciences, SRM University-AP, Amaravati-522503, India.

Corresponding Author: Email: anil.s@srmap.edu.in

Abstract

The integration of nanotechnology into ophthalmology represents a promising frontier for the development of precision diagnostics and therapeutics aimed at enhancing ocular health. While the systemic interactions of iron oxide nanoparticles (IONPs) with blood plasma have been extensively studied, their biomolecular interactions within the ocular environment, particularly human tear, remain largely unexplored. In this study, we comprehensively investigate the physicochemical behaviour and proteomic corona interactions of IONPs upon exposure to human tear extract. Dynamic light scattering (DLS) revealed a modest increase in hydrodynamic diameter from ~115±3.3 nm to ~139±0.7 nm, accompanied by reduction in the zeta potential (ZP) from ~ −36±1.7 mV to ~ −29±1 mV, likely due to protein adsorption. Proteomic profiling v*ia* liquid chromatography–mass spectrometry (LC-MS/MS) identified that 25 tear proteins got adsorbed onto the IONPs when compared to tear alone samples with 91 proteins, revealing the association of Lysozyme C, Lactotransferrin, Mammaglobin B, Lipocalin-1, keratins, immunoglobulins, opiorphin propeptide, Keratin II, Protein S100 and mesothelin proteins implicated in bacteriolysis, iron transport, transcriptional regulation, immune response, cytoskeleton, tissue integrity, nucleotide binding, inflammation regulation, skin tissue formation, endogenous inhibition, microbiome homeostasis and signal transduction. These findings provide protein dynamics of the ocular nano–bio interface, emphasizing the influence of tear protein composition on IONPs. Our results highlight how tear protein corona formation defines the physicochemical stability of IONPs within human tear environment and provide a basic understanding on these alterations which may influence IONP-based ocular therapeutic systems.

Keywords: IONPs, human tear, protein corona signatures, interactions, physicochemical alterations, ocular therapeutics

Significance Statement: Nanomedicine is increasingly being applied to treat ocular diseases, yet while nanoparticle interactions with blood are well-characterized, their behaviour in human tear remain poorly understood. The eye, like the bloodstream, presents a complex and sensitive biological consortium. Herein, we investigated the stability, fate and interactions of IONPs with human tear extract. Through optical and material characterizations, electrophoresis, mass spectrometry and bioinformatic analyses, we revealed the composition and profiling of the tear proteins adsorbed on the IONPs. This study presents an understanding of the IONP–

human tear interactions, providing a foundation for future investigations aimed at the rational design of eye-related nanotherapeutics and diagnostics.

1. Introduction

Nanomedicine is rapidly evolving as a multidisciplinary domain that integrates nanotechnology with medicine to create advanced diagnostics and therapeutics, while enabling the exploration of biological mechanisms beyond traditional pharmaceuticals.[1–3] By utilizing nanomaterials below ~100 nm, researchers can precisely engineer and functionalize nanocargos to achieve superior therapeutic performances.[4–6] These nanosystems facilitate the adsorption and controlled release of high drug payloads, offering prolonged systemic circulation and enhanced delivery to specific organs, tissues, or cellular targets.[7,8] This precision not only boosts therapeutic efficacy but also significantly reduces off-target toxicity and adverse effects.[9,10]

View Article Online
DOI: 10.1039/D5TB02620B

The clinical translation of nanomedicine is well underway, with several FDA-approved nanoformulations already in practice for treating critical conditions such as cancer, antibiotic-resistant infections, chronic inflammation, vaccine delivery and wound care.[7,11] Successful examples include Doxil®, Caelyx®, Abelcet®, Myocet®, and Marqibo® (liposomal drugs); Restasis® (nanoemulsions); Dexferrum®, Venofer® (iron oxide nanoparticles); Feridex® (superparamagnetic iron oxide); Cisplatin® (platinum-based); Hensify® (hafnium oxide); and nanocrystal formulations like Avinza®, Zanaflex®, Tricor®, and Emend®.

The interaction between nanomaterials and biological systems has emerged as a frontier of modern nanomedicine, where materials at the nanoscale interface with the complex biological microenvironment in unexpected and often powerful ways.[12–14] Among the diverse classes of engineered nanostructures, magnetic nanoparticles, *i.e.* IONPs have attracted significant interest due to their unique combination of physicochemical versatility, non-invasive actuation capabilities, and potential for site-specific biointeraction.[15,16] Traditionally applied in targeted drug delivery, Magnetic Resonance Imaging (MRI) contrast enhancement, hyperthermia, and biosensing,[17] IONPs are investigated for their potential in neural stimulation and biophysical modulation of tissues. However, the precise nature of their interactions with neurosensory organs, particularly the eye, remains insufficiently understood.

The complex anatomy and physiology of the human eye present significant challenges in the effective diagnosis and treatment of ocular diseases such as diabetic retinopathy, glaucoma, and age-related macular degeneration. In particular biological barriers like the corneal barrier and the blood–retinal barrier, restricts the efficient delivery of therapeutic agents to target ocular tissues. Even though several nano-formulations have demonstrated encouraging safety and therapeutic efficacy in preclinical animal models, these outcomes have not consistently translated into successful clinical applications in humans[18,19].

A critical factor hindering the clinical translation of ocular nano-formulation is the formation of protein corona, a complex, dynamic layer of adsorbed biomolecules (primarily proteins) that forms almost instantaneously when nanoparticles come in contact with biological fluids such as blood plasma, cerebrospinal or tear.[20,21] This corona alters the "synthetic identity" of the nanoparticle, effectively bestowing it with a biological identity that determines how it is perceived and processed by cells and tissues.[22–24] The composition of the protein corona is influenced by multiple factors including particle size, shape, surface chemistry and charge, as well as the molecular configuration of the biofluids.[25–27] It can drive cellular uptake, modulate immune responses, and activate intracellular signalling cascades depending on the associated protein dominance.[28,29]

View Article Online
DOI: 10.1039/D5TB02620B

While the concept of the protein corona has been extensively studied in oncology, immunology, and drug delivery,[30,31] its implications in sensory neurobiology, particularly within the ocular domain, remain largely unexplored. The eye presents a unique opportunity for investigating corona-mediated interactions, given its accessibility, immune privilege, and sensitivity to micro- and nanoscale perturbations. The corneal epithelium, tear film, and retinal ganglion cells are particularly susceptible to nanoscale stimuli, potentially rendering them responsive to biophysical cues from corona-coated nanoparticles.

In this context, understanding the formation and composition of the protein corona in ocular tear is not merely a physicochemical consideration, but a critical determinant of nanoparticle functionality, biological identity, and therapeutic fate. Despite the growing interest in IONPs for targeted drug delivery and diagnostics, the lack of insight into their interactions within tear presents a significant knowledge gap. Addressing this, in the present study we provide a comprehensive investigation into the physicochemical behaviour and proteomic corona landscape of IONPs in human tear extract. We demonstrate that IONPs undergo a modest increase in hydrodynamic diameter (~115 ± 3.3 nm to ~139 ± 0.7 nm) and a concomitant reduction in surface charge (−36 ± 1.7 mV to −29 ± 1 mV) upon interaction with tear extract, indicative of protein adsorption and surface reconfiguration. Proteomic and bioinformatic analysis revealed protein corona comprising Lysozyme C, Lactotransferrin, Mammaglobin B, Lipocalin-1, various keratins, immunoglobulins, opiorphin propeptide, Keratin II, S100 proteins, and mesothelin. These proteins are functionally associated with diverse biological processes, including bacteriolysis, iron transport, transcriptional regulation, immune response, cytoskeletal organization, tissue integrity, nucleotide binding, inflammation modulation, skin tissue formation, endogenous inhibition, microbiome homeostasis, and signal transduction. Collectively, these findings establish a physicochemical and biomolecular framework for understanding the biotransformation of IONPs within the tear environment, thereby providing critical insights for the rational design of ocular nanotheragnostics.

2. Materials and methods

IONPs of ~30 nm (Product ID: SHP30-02) were purchased from Ocean Nanotech, USA. The particles were supplied as an aqueous dispersion at a concentration of 5 mg/ml. Acrylamide, bisacrylamide, ammonium persulfate, N,N,N′,N′-tetramethylethylenediamine (TEMED), protein molecular weight marker, dithiothreitol (DTT), and Bradford reagent were purchased from Sigma-Aldrich (USA). Schirmer's strips (Whatman filter paper No. 41) were sourced from Madhu Instruments Pvt. Ltd. (India). Transmission electron microscopy (TEM) grids were acquired from Ted Pella Inc. (USA). Human tear samples were collected from healthy adult volunteers at the university clinic by licensed medical personnel. Informed written consent was obtained from all participants after providing detailed instructions regarding the procedure. All other chemicals and reagents were procured from standard commercial suppliers and were of analytical grade or higher.

View Article Online
DOI: 10.1039/D5TB02620B

2. 1 Extraction of human tear proteins

Tear was extracted from 10 healthy volunteers (five females and five males, aged 22–30 years) with no history of contact lens use, dry eye disease, or other ocular abnormalities. To account for biological variability, samples were collected between 9:00 and 11:00 a.m., and were pooled into one sample, under aseptic conditions by a trained ophthalmic professional. Similarly, two additional biological replicates were collected over the following two consecutive days, with one replicate obtained per day. These biological triplicates were used for all experiments, including DLS, zeta potential, and LC-MS/MS analyses. Briefly, Schirmer's strip was bent at the zero mark to form an angle of 120º and gently placed under the lower eyelid until the tear front reached the 30 mm mark. The strips were then carefully removed and cut into uniform segments of 5 mm length. These segments were incubated in 100 µl of 100 mM ammonium bicarbonate (NH_4HCO_3) buffer (pH 7.8) at 4 °C for 1 hour to facilitate the release of tear proteins into the buffer. After incubation, the strip pieces were removed using sterile forceps, and the resulting supernatant containing the tear was collected and stored at 4 °C for subsequent analyses. Ethical approval for human tear sample collection was obtained from the Institutional Ethics Committee (IEC), SRM University-AP (Ref. No. SRMAP/IEC/2025-15; Application No. IEC-15). All procedures were conducted in accordance with the ethical standards of the institutional research committee and applicable national guidelines. Written informed consent was obtained from all participants prior to tear collection.

2. 2 Human tear protein corona formation on IONPs

IONPs were incubated with the extracted human tear extract in 100 mM ammonium bicarbonate (37 °C, pH 7.8) for 1 hour to facilitate the gradual adsorption of tear proteins onto the IONP surface, leading to the formation of a tear protein corona-IONP complex (IONP@TPC).

2. 3 Assessment of stability, dispersity, and integrity of IONP@TPC

The progression of protein binding to the IONPs over time was monitored using DLS, and ZP measurements at a concentration of ~200 µM in Milli Q water (neutral pH) at 25 °C. Hydrodynamic diameter was determined using

a backscattering angle of 173° in a low-volume glass cuvette (12 µl). ZP measurements were performed using a clear disposable folded capillary cell. These analyses were used to evaluate nanoparticle dispersity, colloidal stability, and surface charge changes following protein corona formation. All experiments were performed in triplicates to ensure reproducibility and the data are expressed as mean values ± standard deviation (SD).

FTIR analysis was performed in attenuated total reflectance (ATR) mode using a Bruker Alpha II spectrometer to investigate proteinaceous functional groups and biochemical signatures associated with tear protein corona formation on IONPs. Samples of IONPs alone and IONP@TPC were prepared in Milli Q water, drop-cast onto clean glass slides, air-dried according to standard FTIR preparation protocols, and analyzed between the wavenumbers of 500 cm^{-1} to 3500 cm^{-1}.

View Article Online
DOI: 10.1039/D5TB02620B

TEM was employed to assess nanoparticle morphology and structural integrity before and after corona formation by drop-casting the samples onto carbon-coated copper grids, followed by drying at room temperature. Negative staining with 2% uranyl acetate was performed to enhance contrast and enable visualization of the protein corona surrounding the IONPs. Together, these complementary techniques comprehensively evaluated the IONPs stability, dispersity, and integrity following interaction with tear extract proteins.

2. 4 Isolation and identification of tear protein corona associated with the IONPs

Following incubation, the IONP@TPC complexes were isolated by centrifugation and washed thoroughly to remove the unbound proteins. To dissociate the adsorbed tear proteins from the surface of the IONPs, the particles were first washed four times with 100 mM ammonium bicarbonate buffer (NH_4HCO_3, pH 7.8) *via* centrifugation at 16,000 × g for 10 minutes to eliminate loosely bound (soft corona) or unbound proteins. Subsequently, 3 µl of 100 mM dithiothreitol (DTT) and 7 µl of 2× Laemmli sample buffer was added to the IONP@TPC pellet, resulting in a final DTT concentration of 30 mM, followed by incubation at 95 °C for 15 minutes to induce protein desorption as indicated by nanoparticle aggregation. The aggregated IONPs were then centrifuged at 16,000 × g for 5 minutes, and the resulting supernatant, containing the released corona proteins from the IONPs, were collected and stored at 4 °C for further analysis using SDS-Polyacrylamide Gel Electrophoresis (SDS-PAGE) and mass spectrometry. The total protein concentration of pooled tear samples and wash fractions was quantified using the Bradford assay. Equal amounts of quantified protein samples were subsequently loaded into each well to ensure consistency and uniformity across all analyses.

SDS-PAGE of tear extract controls and unbound or loosely bound (soft corona) proteins and the IONP extracted proteins, 10 µl of each protein samples were mixed separately with 10 µl of 2× Laemmli buffer (Invitrogen) and heated at 95 °C for 5 minutes to ensure complete protein denaturation. The prepared samples, along with 2 µl of Benchmark™ pre-stained protein molecular weight ladder (Invitrogen), were loaded onto a 12% Tris-polyacrylamide gel and electrophoresed in Tris-glycine running buffer (Invitrogen) at 120 V for 45

minutes. Following electrophoresis, the gel was fixed overnight in a solution containing 10% (v/v) acetic acid and 40% (v/v) ethanol. Protein bands were then visualized by staining with Coomassie Brilliant Blue R-250, and excess stain was removed by de-staining using 10% (v/v) methanol and 10% (v/v) acetic acid. Gel images were captured using Gel Doc XR+ system, Bio-Rad**.** The electrophoretic analysis was intended to qualitatively compare the protein profiles and monitor the removal of loosely bound or unbound proteins during the washing steps.

2. 5 LC-MS/MS measurements and bioinformatics analysis

For LC-MS/MS analysis, protein samples were resolved by SDS-PAGE and visualized using Coomassie staining. Protein bands were carefully excised using a clean scalpel under sterile conditions as instructed by the proteomics facility of Rajiv Gandhi Centre for Biotechnology (RGCB). The gel pieces were transferred into sterile 1.5 mL microcentrifuge tubes containing 50% methanol to maintain hydration and sample stability. To avoid contamination, all the samples were prepared using fresh reagents, autoclaved Milli -Q water, and detergent-free glassware. The samples were subjected to in-gel digestion and label-free quantitative (LFQ) proteomics analysis. Workflow-matched blank control of IONPs without tear extract was processed under identical conditions to evaluate background contamination. The processed output was provided as excel files containing identified proteins along with their corresponding UniProt IDs, unique peptides, peptide count and normalized abundance values. The dataset was further curated by applying standard filtering criteria (unique peptides ≥ 1 and peptide count ≥ 2), and proteins consistently identified across biological replicates were retained for downstream analysis. To correct for technical variability, raw protein abundance values were normalized and were $\log_2$-transformed prior to further analysis. Using these processed data, heatmaps were generated using TBtools software, and ExPASy Compute pI/Mw tool (https://web.expasy.org/compute_pi/) was used to calculate theoretical isoelectric points and molecular weights of the proteins. Protein–protein interaction analysis was performed using the STRING database (version 12.0, https://string-db.org) with Markov Cluster Algorithm (MCL) clustering. Gene Ontology (GO) analysis (Biological Process) was conducted using STRING, and the top ten functional categories were selected based on false discovery rate (FDR ≤ 0.05). All analyses were performed using established bioinformatics tools and standard parameters to ensure consistency and reproducibility.

2. 6 Material characterizations

Solution-phase absorption spectra of IONPs and IONP@TPC complexes were recorded using a Thermo Multiskan Sky spectrophotometer in standard 96-well plates, with a wavelength resolution of 1 nm. Dynamic light scattering (DLS) and zeta potential (ZP) measurements were performed using a Zetasizer system (Malvern Instruments, NY, USA). High-resolution transmission electron microscopy (HR-TEM) samples were prepared by drop-casting 5 µl of nanoparticle suspensions onto carbon-coated copper TEM grids. Negative staining was performed to enhance contrast, enabling the assessment of morphological characteristics of IONPs before and

after tear protein corona formation. Images were captured using a JEOL JEM-2100 PLUS transmission electron microscope (JEOL, Japan).

3. Results and discussion

IONPs have emerged as promising nanocargos in nanomedicine, offering unique magnetic, catalytic, and imaging properties that pave the way for advanced therapeutic and diagnostic strategies across various diseases, including complex and life-threatening conditions such as cancer. With systemic delivery typically involving blood circulation, extensive research has explored the interactions of IONPs with blood components, including erythrocytes, plasma proteins, and immune cells.[32,33] Recently, the applications of nanomedicine have been rapidly expanding into the field of ophthalmology, where IONPs present innovative opportunities for the treatment and diagnosis of ocular disorders. Despite this progress, the interaction between IONPs and human tear extract, an essential biological barrier in ocular drug delivery, remains undiscovered. Our study delves into this critical yet understudied aspect, aiming to understand the interaction of IONPs with protein biomolecular consortium of human tear extract, so as to aid rational designing of IONP-based theragnostic platforms tailored for ophthalmic implementations in future.

View Article Online
DOI: 10.1039/D5TB02620B

To investigate these interactions, we employed monodispersed IONPs as our model nanocargo, given their widespread use in biomedical applications and their progression toward clinical approval due to favorable biocompatibility and imaging capabilities. Human tear extract was incubated with IONPs for 1 hour to study particles stability and surface transformations. Following incubation, the IONPs were subjected to thorough washing steps to eliminate unbound or weakly adsorbed proteins. The resulting IONP@TPC complexes were initially analyzed using advanced material characterizations to evaluate colloidal stability, physicochemical changes, and surface modifications. To elucidate the identity and potential functions of the adsorbed tear proteins, the tightly bound protein corona was extracted using DTT at 95 °C (see Methods Section for details), followed by analyses using SDS-PAGE, mass spectrometry and proteomics (Fig. 1).

To validate the stability of the IONP@TPC (Fig. 3e, g), we compared their TEM images with those of pristine IONPs (Fig. 3d, f). Given the monodispersity and small size of the IONPs (~27 ± 2 nm), accurately measuring the thickness of the tear protein corona surrounding them is inherently challenging. Therefore, we acquired multiple HR-TEM images across various regions of the grid upon negative staining (Fig. S1). TEM imaging of the negatively stained IONP@TPC revealed a distinct, though relatively uniform, proteinaceous layer encasing the electron-dense IONPs. This appeared as a characteristic white brim or halo surrounding the IONPs (Fig. 3e), which lacked in IONPs controls with no protein adsorption (Fig. 3d).

Stability is a critical determinant for the effective functionalization of nanoparticles in therapeutic, diagnostic, imaging, and drug delivery applications, where preserving interaction integrity in aqueous biological environments is essential. Statistical analysis of size distribution, performed by evaluating at least 100 individual particles (Fig. 3g), revealed an increase in the average diameter from ~27±2 nm to ~31±3 nm upon TPC formation. Interestingly, the observed protein layer appeared uneven, contrasting with previous reports of a consistent ~5 nm corona formed around 500 nm silica particles incubated with blood plasma.[34] This deviation is likely attributable to the nanoscale size of IONPs and their distinct surface curvature, which influence protein adsorption dynamics.

View Article Online
DOI: 10.1039/D5TB02620B

Such inconsistencies echo the analytical complexities often encountered in other biologically relevant systems, such as catalytic degradation reactions or radical trapping studies, where surface phenomena are highly sensitive to nanoscale interactions and fluid composition.[35]

While the IONPs retained their colloidal stability, a gradual increase in hydrodynamic diameter from 115±3.3 nm (0.2 poly dispersity index (PDI)) to 139±0.7 nm (0.3 PDI) was observed when treated for 1 h with human tear extract (Fig. 2c, Table 1). The average diameter initially increased from 115±3.3 nm to 200±5 nm at 15 min and then decreased progressively to 150±1 nm at 30 min, and to 147±2 nm at 45 min (Fig. 2c). This temporal evolution was further supported by ZP measurements, where the surface charge of IONPs reduced from −36±1.7 mV to −31±0.1 mV within the first 15 minutes, subsequently stabilizing at −29±1 mV by 60 minutes (Fig. 2d, Table 1). This behaviour may reflect the initial association of random tear proteins onto the nanoparticle surface, followed by gradual replacement by proteins with comparatively higher surface affinity over time, resulting in the association of relatively stable proteins. Such temporal adsorption behaviour is consistent with the classical Vroman effect, where initially adsorbed proteins are dynamically exchanged by more strongly interacting proteins.[36]

To gain deeper insights into the formation of the TPC around IONPs, FTIR spectra of IONPs and IONP@TPC samples were compared (Fig. 2b), which provided substantial evidence for the adsorption of tear proteins. While both IONPs and IONP@TPC exhibited characteristic peaks for C–H vibrations, atmospheric CO_2, Fe–carbonyl, C=O, and Fe–O stretching at 2925 cm^{-1}, 2857 cm^{-1}, 2351 cm^{-1}, 2144 cm^{-1}, 1958 cm^{-1} and 583 cm^{-1}, the presence of additional peaks at 1538 cm^{-1} and 1397 cm^{-1} in IONP@TPC likely due to protein-derived amide II and NH_4^+ group vibrations. Furthermore, the observed red shifts in amide I (1695 $cm^{-1} \rightarrow$ 1639 cm^{-1}) and C–N vibrations (1117 $cm^{-1} \rightarrow$ 1036 cm^{-1}) suggest hydrogen bonding and structural rearrangement of protein motifs implying binding. These spectral features are indicative of protein corona formation and substantiate protein–IONP interaction at the molecular level.

Electrophoresis analyses were performed immediately after incubation of IONPs with human tear extract, following 1 hour of interaction, and after sequential purification steps to remove any unbound or loosely bound

proteins. Initially, the electrophoretic protein band profiles of the IONP@TPC samples resembled those of the untreated tear extract controls. However, with each successive washing step, loosely associated proteins were progressively eliminated. After the first wash, the protein pattern remained comparable to the control tear extract (Fig. 3a, L3). The second wash revealed a reduced set of persistent proteins (Fig. 3a, L4), while the third wash showed only minimal residual bands (Fig. 3a, L5). By the fourth wash, no detectable protein bands were observed (Fig. 3a, L6), indicating that all loosely bound proteins had been effectively removed, leaving behind only the strongly adsorbed proteins on the IONPs. This trend was further corroborated by protein quantification using the Bradford Assay (Fig. 3c), suggesting the retention of a tightly bound, stable protein layer on the IONPs.

View Article Online
DOI: 10.1039/D5TB02620B

To further investigate the tightly bound proteins associated with the IONPs, we isolated the nanoparticle–bound protein by treating IONP@TPC with 30 mM dithiothreitol (DTT) at 95 °C. This process disrupted disulfide linkages and facilitated the solubilization of adsorbed protein fragments. The IONPs were subsequently separated by repeated centrifugation at 16,000 g, and the resulting supernatant containing the desorbed proteins were subjected to SDS-PAGE followed by spectrometry. The electrophoretic profiles revealed that the proteins retained molecular weights in the range of 100 kDa to 6.5 kDa like their native forms present in untreated tear extract samples (Fig. 3a and b). Notable differences in band intensities between the IONP@TPC samples and the tear extract indicating comparatively low protein recovery in the corona fraction, suggest that only a limited subset of tear proteins became associated with the nanoparticle surface, potentially reflecting differential affinity-driven interactions.

Interestingly, contrasting results have been reported for 9 nm silica (Si) nanoparticles incubated with blood plasma, where an increase in protein concentration surrounding the particles indicated preferential adsorption.[37] Similar interactions were also observed by Chuan Wang et. al., who analyzed the intracellular protein corona of AuNPs.[38] Their findings highlighted the association of proteins involved in nanoparticle internalization and trafficking, particularly implicating clathrin-mediated endocytosis. Once internalized, these nanoparticles undergo endo-lysosomal processing, which can further modulate their biological identity and function.

Further, proteomic analysis was conducted to identify the proteins that are associated with the IONPs. All bands corresponding to the IONP@TPC (Fig. 3b, L3) and the complete tear extract controls (Fig. 3b, L2) from the SDS-PAGE gel were excised, enzymatically digested with trypsin, and analyzed *via* liquid chromatography–tandem mass spectrometry (LC-MS/MS) (Fig. 4 and Table 2). In addition, workflow-matched blanks (tear extract untreated IONPs) were processed under identical conditions and subjected to LC–MS/MS analysis to assess background contributions. Blank controls showed the presence of a limited number of low-abundance proteins, primarily arising from sample processing and LC–MS/MS workflows, including trypsin autolysis products and common keratin contaminants) (Table S1). Such background signals are widely reported in proteomic analyses

and are attributed to proteolytic enzyme carryover and environmental contamination during sample handling and preparation (e.g., skin- and dust-derived keratins). Most common contaminants that are usually detected in the blank controls are keratins (KRT1, KRT10, KRT9, KRT2, KRT47, KRT5, KRT14, KRT6F, and KRT6A)[39].

For instance, KRT1 and KRT9, identified in both IONP@TPC and negative controls, are reported as common environmental and sample-processing contaminants in tear extract[39]. Similarly, KRT75, a hair follicle-associated epithelial keratin, is considered a potential environmental contaminant in tear proteomic studies and may arise from incidental eyelash contact during Schirmer strip collection[39]. In contrast, KRT3 is a physiologically relevant corneal epithelium-keratin involved in maintaining corneal epithelial integrity and barrier function, thereby contributing to ocular surface protection[39]. Even though keratins and certain other proteins were detected in the workflow-matched blank controls presumably due to handling or workflow contributions, they remained consistent in the IONP@TPC across triplicates. Therefore, they were retained for downstream analyses as possible corona-associated proteins. However, their origin cannot be unequivocally assigned to the protein corona and any functional interpretations involving these proteins should be considered with caution. Further studies are needed to clarify their contribution to corona composition and associated biological functions.

View Article Online
DOI: 10.1039/D5TB02620B

Comprehensive proteomic profiling revealed a distinctive set of proteins that got associated with IONPs, as visualized by hierarchical clustering (Fig. 4a). The heatmap indicates variations in protein abundance patterns between tear extract and IONP@TPC. In the tear extract sample, Lipocalin and Lysozyme C were among the most abundant proteins, whereas in the IONP@TPC, Lysozyme C and Lactotransferrin were prominently observed. Notably, Lactotransferrin is a known metal-binding protein, suggesting that protein physicochemical properties may contribute to their association with the nanoparticle surface (Table 2). This trend was further substantiated by the Venn diagram (Fig. 4b), revealing 91 proteins in the tear extract and 25 consistently found proteins in the IONP@TPC across all the triplicates whereas the remaining 66 proteins exhibited either no binding or inconsistent association across replicates (Table S2).

GRAVY score analysis (Fig. 4c) showed high proportion of hydrophilic proteins associated with the IONP@TPC, with only 3 of the 25 identified proteins exhibiting hydrophobic characteristics. Hydrophobic nanoparticle surfaces are known to preferentially adsorb opsonin proteins, promoting rapid opsonization and phagocytic clearance,[40,41] whereas hydrophilic surfaces, as extensively demonstrated for polyethylene glycol (PEG), hydrophilic polymer, are associated with a comparatively favourable biological interface. Therefore, the predominance of hydrophilic proteins in the corona is presumably advantageous for improving colloidal stability and circulation behavior.[42]

Moreover, analysis of the molecular weight (MW) and isoelectric point (pI) distributions (Fig. 4d, e) revealed that IONPs adsorbed low molecular weight proteins (~10–20 kDa range), with pI values between 5 and

6, despite the negatively charged nature of the IONPs, the adsorption of these relatively acidic proteins may occur through localized electrostatic interactions involving cationic surface patches, counterion screening at a near physiological pH.[43] Although relatively acidic proteins constituted a larger number of the adsorbed proteome, positively charged proteins (Lysozyme C, Lactotransferrin) appeared to dominate the corona composition.

Alongside, proteins such as Proline-rich protein 4, Prolactin-inducible protein, and extracellular glycoprotein lacritin were also observed on the IONP surface, indicating associations with retina homeostasis, tissue homeostasis, and general homeostatic processes, suggesting that the protein composition reflects physiological roles in maintaining cellular and tissue balance. (Fig. 5 and Table S3). This newly acquired biological identity not only stabilizes the nanoparticle interface but may also influence its physiological fate, including biodistribution, immune recognition, and therapeutic performance. Protein corona formation is increasingly recognized as a central determinant of nanoparticle behaviour *in vivo*, where it can mask engineered surface functionalities, alter targeting efficiency, and modulate clearance pathways. In systemic nanomedicine, uncontrolled corona formation has been associated with opsonization and rapid immune uptake, whereas strategic understanding and modulation of corona composition enhances circulation time and therapeutic specificity. Accordingly, mapping the tear-protein corona from IONPs extends beyond ocular relevance and contributes to the broader framework of designing bio-interactive and translationally robust nanotherapeutic platforms.[44]

Comprehensive protein–protein interaction and functional analyses of the IONP@TPC revealed a biologically relevant protein profile. In the STRING-based network analysis, tear extract dataset (Fig. 5a) showed multiple interconnected protein groups related to retina homeostasis, intermediate filament organisation, immunoglobulin complex, metabolism of xenobiotics by cytochrome P450, whereas the IONP@TPC dataset (Fig. 5b) also retained a subset of these proteins,, primarily corresponding to retina homeostasis and intermediate filament organisation. This distribution reflects the presence of functionally related proteins and provides a biological context for the identified protein composition.

Further analysis using Biological Process (Gene Ontology (GO)) highlighted the presence of proteins related to retina homeostasis, tissue homeostasis, homeostatic process, and intermediate filament organization, common to tear extract (Fig. 5c) and IONP@TPC (Fig. 5d) in the top 10 functional categories, reflecting the retention of key functional categories. The complete set of functional categories for both tear extract and IONP@TPC is provided in the Supporting Information (Table S4 and Table S5). Importantly, a subset of associated proteins was linked to humoral immune responses, antimicrobial defense, fungal defense, and cytotoxic activity. This is consistent with previous reports showing that protein coronas can carry immunologically active signatures that modulate nanoparticle clearance, inflammation, or tissue targeting.[47,48] However, the precise reason for the association of these proteins with the nanoparticle surface remains unclear.

Furthermore, the potential cellular uptake behaviour and immunological responses triggered by this corona composition are being explored as future studies.

We have ongoing investigations aimed at systematically evaluating the influence of nanoparticle-specific parameters, including core composition (e.g., IONPs *vs* liposomes), size, shape, surface functionalization, and incubation duration on their interactions with human tear extract. These studies are focused on elucidating the biocompatibility, therapeutic performance, cellular processing, and the dynamic transformation of the IONP@TPC. Having now identified the tear proteins with critical biological functions that get associated with IONPs, our future efforts will explore how such interactions impact the endogenous bioactivity of randomly selected proteins, with significant biological function, providing deeper insight into the futuristic consequences of protein corona formation in the context of ophthalmic nanomedicine.

View Article Online
DOI: 10.1039/D5TB02620B

Conclusions

This study explores the pivotal yet underexamined interaction between IONPs and human tear extract, representing a foundational step toward advancing nanomedicine in ophthalmology. As IONPs gain prominence in ocular diagnostics, imaging, and therapy, understanding their behavior in the tear film microenvironment is essential to preserve their therapeutic efficacy while minimizing unintended biological interference. Our findings demonstrate that IONPs can retain colloidal stability in the presence of human tear extract, resisting aggregation (Fig. S1) while exhibiting an average increase of hydrodynamic diameter from ~115±3.3 to 139±0.7 nm, indicating protein corona formation. Zeta potential measurements revealed a notable shift in the surface charge from –36±1.7 mV to –29±1 mV, reflecting charge modulation due to adsorbed tear proteins. Proteomic and LC–MS/MS analysis identified 91 proteins in the tear extract, of which 25 proteins were consistently found to be associated with the IONPs. Bioinformatic analysis revealed the association of functionally diverse proteins, including Lysozyme C, Lactotransferrin, Mammaglobin B, Lipocalin-1, keratins, immunoglobulins, opiorphin propeptide, Keratin II, S100 proteins, and mesothelin. Collectively, these proteins have a role in bacteriolysis, iron transport, transcriptional regulation, immune modulation, cytoskeletal organization, tissue integrity, nucleotide binding, inflammation control, epithelial and skin tissue formation, endogenous inhibition, microbiome homeostasis, and signal transduction. This work offers a comprehensive profiling of the tear protein corona on IONPs, delivering critical insights into how IONP physicochemical properties are influenced by human tear extract. These insights are essential for designing next-generation ophthalmic nanomedicines that not only retain their functional properties but also harmonize with the exogenous ocular proteome, ultimately paving the way for safer, targeted, and more effective treatment options for a wide range of ocular disorders.

Data availability

No data was used from an external source. All the LC-MS/MS data is deposited at zenodo having a DOI number of 10.5281/zenodo.19401485.

Supporting Information

The Supporting Information is available free of charge at www.rsc.org

Transmission electron microscopy (TEM) images of pristine IONP and protein corona–adsorbed iron oxide nanoparticles (IONP@TPC). Proteins detected in LC–MS/MS workflow-matched blanks (IONPs without tear extract) processed under identical conditions. Table illustrating all the proteins identified in human tear extract. Biological Functions of Proteins identified in IONP@TPC. Functional category of proteins identified in tear extract based on Gene Ontology analysis. Functional category of proteins identified in IONP@TPC based on Gene Ontology analysis.

Author contributions

A. K. S., conceived the idea, planned and designed the research and experiments, analyzed and interpreted the results, and wrote the manuscript (MS); B.P., performed all the experiments and characterizations, analyzed and interpreted the data, out-sourcing work, gathered necessary literature and prepared the images and tables for the MS; S.A., assisted B.P., in performing all the experiments, characterizations, and gathering references.

Acknowledgements

The authors thank SCIF and NRC, SRMIST, Chennai for instrument characterizations. LC-MS/MS measurements are a courtesy of the central proteomic research facility of RGCB. The authors also thank the Instrumentation Research Facility of SRM-AP.

References

1 W. Lin, *Chem. Rev.*, 2015, **115**, 10407–10409.
2 N. F. Attia, E. M. A. El-Monaem, H. G. El-Aqapa, S. E. A. Elashery, A. S. Eltaweil, M. El Kady, S. A. M. Khalifa, H. B. Hawash and H. R. El-Seedi, *Appl. Surf. Sci. Adv.*, 2022, **11**, 100284.
3 E. C. Dreaden, A. M. Alkilany, X. Huang, C. J. Murphy and M. A. El-Sayed, *Chem. Soc. Rev.*, 2012, **41**, 2740–2779.
4 M. J. Mitchell, M. M. Billingsley, R. M. Haley, M. E. Wechsler, N. A. Peppas and R. Langer, *Nat. Rev. Drug Discov.*, 2021, **20**, 101–124.
5 P. K. Hashim and S. S. M. A. Abdrabou, *Nanoscale Horiz.*, 2024, **9**, 693–707.
6 X. Cheng, Q. Xie and Y. Sun, *Front. Bioeng. Biotechnol.*, DOI:10.3389/fbioe.2023.1177151.
7 R. Tenchov, K. J. Hughes, M. Ganesan, K. A. Iyer, K. Ralhan, L. M. Lotti Diaz, R. E. Bird, J. M. Ivanov and Q. A. Zhou, *ACS Nano*, 2025, **19**, 4011–4038.
8 P.-D. Ly, K.-N. Ly, H.-L. Phan, H. H. T. Nguyen, V.-A. Duong and H. V. Nguyen, *Front. Nanotechnol.*, DOI:10.3389/fnano.2024.1456939.
9 D. Fan, Y. Cao, M. Cao, Y. Wang, Y. Cao and T. Gong, *Signal Transduct. Target. Ther.*, 2023, **8**, 293.
10 C. Oh, H. N. Jung, J. Park, J. M. Awad, D. Jiang, D. J. Dowling and H.-J. Im, *ACS Nano*, DOI:10.1021/acsnano.5c04836.
11 R. Tenchov, R. Bird, A. E. Curtze and Q. Zhou, *ACS Nano*, 2021, **15**, 16982–17015.
12 X. Tian, Y. Chong and C. Ge, *Front. Chem.*, DOI:10.3389/fchem.2020.00446.
13 Y. Fu, T. Liu, H. Wang, Z. Wang, L. Hou, J. Jiang and T. Xu, *J. Sci. Adv. Mater. Devices*, 2024, **9**, 100694.
14 H. Zhao, Y. Wang, L. Bao and C. Chen, *Acc. Mater. Res.*, 2022, **3**, 812–829.
15 Z. Ma, J. Mohapatra, K. Wei, J. P. Liu and S. Sun, *Chem. Rev.*, 2023, **123**, 3904–3943.
16 S. Mishra and M. D. Yadav, *Langmuir*, 2024, **40**, 17239–17269.
17 Kritika and I. Roy, *Mater. Adv.*, 2022, **3**, 7425–7444.
18 G. A. Rodrigues, D. Lutz, J. Shen, X. Yuan, H. Shen, J. Cunningham and H. M. Rivers, *Pharm. Res.*, 2018, **35**, 245.
19 S. Soares, J. Sousa, A. Pais and C. Vitorino, *Front. Chem.*, DOI:10.3389/fchem.2018.00360.
20 Transcranial static magnetic field stimulation over hMT+ inhibits visual motion discriminability | Scientific Reports, https://www.nature.com/articles/s41598-023-51097-x, (accessed July 4, 2025).
21 L. Cervetto, G. C. Demontis and C. Gargini, *Br. J. Pharmacol.*, 2007, **150**, 383–390.
22 What the Cell "Sees" in Bionanoscience | Journal of the American Chemical Society, https://pubs.acs.org/doi/10.1021/ja910675v, (accessed July 4, 2025).
23 K. Obst, G. Yealland, B. Balzus, E. Miceli, M. Dimde, C. Weise, M. Eravci, R. Bodmeier, R. Haag, M. Calderón, N. Charbaji and S. Hedtrich, *Biomacromolecules*, 2017, **18**, 1762–1771.
24 A. Amici, D. Pozzi, C. Marchini and G. Caracciolo, *Mol. Pharm.*, 2023, **20**, 5247–5253.
25 Size-Dependent Protein–Nanoparticle Interactions in Citrate-Stabilized Gold Nanoparticles: The Emergence of the Protein Corona | Bioconjugate Chemistry, https://pubs.acs.org/doi/10.1021/acs.bioconjchem.6b00575, (accessed July 4, 2025).
26 R. Madathiparambil Visalakshan, L. E. González García, M. R. Benzigar, A. Ghazaryan, J. Simon, A. Mierczynska-Vasilev, T. D. Michl, A. Vinu, V. Mailänder, S. Morsbach, K. Landfester and K. Vasilev, *Small*, 2020, **16**, 2000285.
27 W. Wang, Z. Huang, Y. Li, W. Wang, J. Shi, F. Fu, Y. Huang, X. Pan and C. Wu, *Acta Pharm. Sin. B*, 2021, **11**, 1030–1046.
28 C. C. Fleischer and C. K. Payne, *Acc. Chem. Res.*, 2014, **47**, 2651–2659.
29 Y. Yan, K. T. Gause, M. M. J. Kamphuis, C.-S. Ang, N. M. O'Brien-Simpson, J. C. Lenzo, E. C. Reynolds, E. C. Nice and F. Caruso, *ACS Nano*, 2013, **7**, 10960–10970.
30 Impact of Protein Corona Formation on the Thermoresponsive Behavior of Acrylamide-Based Nanogels | Biomacromolecules, https://pubs.acs.org/doi/10.1021/acs.biomac.3c01405, (accessed July 4, 2025).
31 D. Chakraborty, K. R. Ethiraj and A. Mukherjee, *RSC Adv.*, 2020, **10**, 27161–27172.
32 Y. Portilla, V. Mulens-Arias, N. Daviu, A. Paradela, S. Pérez-Yagüe and D. F. Barber, *ACS Appl. Mater. Interfaces*, 2023, **15**, 35906–35926.
33 H. Arami, A. Khandhar, D. Liggitt and K. M. Krishnan, *Chem. Soc. Rev.*, 2015, **44**, 8576–8607.
34 S. Tenzer, D. Docter, S. Rosfa, A. Wlodarski, J. Kuharev, A. Rekik, S. K. Knauer, C. Bantz, T. Nawroth, C. Bier, J. Sirirattanapan, W. Mann, L. Treuel, R. Zellner, M. Maskos, H. Schild and R. H. Stauber, *ACS Nano*, 2011, **5**, 7155–7167.
35 C. Wang, B. Chen, M. He and B. Hu, *ACS Nano*, 2021, **15**, 3108–3122.
36 L. Vroman and A. L. Adams, *J. Biomed. Mater. Res.*, 1969, **3**, 43–67.
37 The Evolution of the Protein Corona around Nanoparticles: A Test Study | ACS Nano, https://pubs.acs.org/doi/10.1021/nn202458g, (accessed July 4, 2025).
38 C. Wang, B. Chen, M. He and B. Hu, *ACS Nano*, 2021, **15**, 3108–3122.

39 S. Ahmed, J. Altman, G. Jones, T. J. Lee, D. M. Robertson, W. Zhi, S. Sharma and A. Sharma, *Exp. Eye Res.*, 2025, **251**, 110231.
40 H. Carrstensen, R. H. Müller and B. W. Müller, *Clin. Nutr.*, 1992, **11**, 289–297.
41 R. H. Müller, K. H. Wallis, S. D. Tröster and J. Kreuter, *J. Controlled Release*, 1992, **20**, 237–246.
42 *Int. J. Pharm.*, 2006, **307**, 93–102.
43 How Negatively Charged Proteins Adsorb to Negatively Charged Surfaces: A Molecular Dynamics Study of BSA Adsorption on Silica | The Journal of Physical Chemistry B, https://pubs.acs.org/doi/10.1021/acs.jpcb.6b07646, (accessed February 6, 2026).
44 A. K. Barui, J. Y. Oh, B. Jana, C. Kim and J.-H. Ryu, *Adv. Ther.*, 2020, **3**, 1900124.
45 M. P. Monopoli, D. Walczyk, A. Campbell, G. Elia, I. Lynch, F. Baldelli Bombelli and K. A. Dawson, *J. Am. Chem. Soc.*, 2011, **133**, 2525–2534.
46 M. Lundqvist, J. Stigler, G. Elia, I. Lynch, T. Cedervall and K. A. Dawson, *Proc. Natl. Acad. Sci.*, 2008, **105**, 14265–14270.
47 A. Salvati, A. S. Pitek, M. P. Monopoli, K. Prapainop, F. B. Bombelli, D. R. Hristov, P. M. Kelly, C. Åberg, E. Mahon and K. A. Dawson, *Nat. Nanotechnol.*, 2013, **8**, 137–143.
48 M. J. Hajipour, S. Laurent, A. Aghaie, F. Rezaee and M. Mahmoudi, *Biomater. Sci.*, 2014, **2**, 1210–1221.
49 T. Cedervall, I. Lynch, S. Lindman, T. Berggård, E. Thulin, H. Nilsson, K. A. Dawson and S. Linse, *Proc. Natl. Acad. Sci.*, 2007, **104**, 2050–2055.
50 S. Tenzer, D. Docter, J. Kuharev, A. Musyanovych, V. Fetz, R. Hecht, F. Schlenk, D. Fischer, K. Kiouptsi, C. Reinhardt, K. Landfester, H. Schild, M. Maskos, S. K. Knauer and R. H. Stauber, *Nat. Nanotechnol.*, 2013, **8**, 772–781.
51 J. Kumar, W. Weber, S. Münchau, S. Yadav, S. B. Singh, K. Saravanan, M. Paramasivam, S. Sharma, P. Kaur, A. Bhushan, A. Srinivasan, C. Betzel and T. P. Singh, *Indian J. Biochem. Biophys.*, 2003, **40**, 14–21.
52 D. P. Dickinson and M. Thiesse, *Invest. Ophthalmol. Vis. Sci.*, 1995, **36**, 2020–2031.
53 J. Schaller, K. Akiyama, H. Kimura, D. Hess, M. Affolter and E. E. Rickli, *Eur. J. Biochem.*, 1991, **196**, 743–750.
54 Human oral lectin ZG16B acts as a cell wall polysaccharide probe to decode host–microbe interactions with oral commensals | PNAS, https://www.pnas.org/doi/10.1073/pnas.2216304120, (accessed April 1, 2026).
55 N.-N. Chuang and C.-C. Huang, *Biochem. Soc. Trans.*, 2007, **35**, 1292–1294.
56 G. Teng and F. N. Papavasiliou, *Annu. Rev. Genet.*, 2007, **41**, 107–120.
57 H. W. Schroeder and L. Cavacini, *J. Allergy Clin. Immunol.*, 2010, **125**, S41–S52.
58 C. Champaiboon, K. J. Sappington, B. D. Guenther, K. F. Ross and M. C. Herzberg, *J. Biol. Chem.*, 2009, **284**, 7078–7090.
59 A. Wisner, E. Dufour, M. Messaoudi, A. Nejdi, A. Marcel, M.-N. Ungeheuer and C. Rougeot, *Proc. Natl. Acad. Sci.*, 2006, **103**, 17979–17984.
60 S. Kobayashi, S. Kore-eda and T. Tanaka, *FEBS Lett.*, 1999, **447**, 39–43.
61 Mutations in cornea-specific keratin K3 or K12 genes cause Meesmann's corneal dystrophy | Nature Genetics, https://www.nature.com/articles/ng0697-184, (accessed April 1, 2026).
62 H. W. Schroeder and L. Cavacini, *J. Allergy Clin. Immunol.*, 2010, **125**, S41–S52.
63 M. Røe, I. N. Norderhaug, P. Brandtzaeg and F. E. Johansen, *J. Immunol.*, 1999, **162**, 6046–6052.
64 T. Rogalla, M. Ehrnsperger, X. Preville, A. Kotlyarov, G. Lutsch, C. Ducasse, C. Paul, M. Wieske, A.-P. Arrigo, J. Buchner and M. Gaestel, *J. Biol. Chem.*, 1999, **274**, 18947–18956.
65 J.-C. Simard, D. Girard and P. A. Tessier, *J. Leukoc. Biol.*, 2010, **87**, 905–914.
66 M. McHeyzer-Williams, S. Okitsu, N. Wang and L. McHeyzer-Williams, *Nat. Rev. Immunol.*, 2012, **12**, 24–34.

Figures

Figure 1

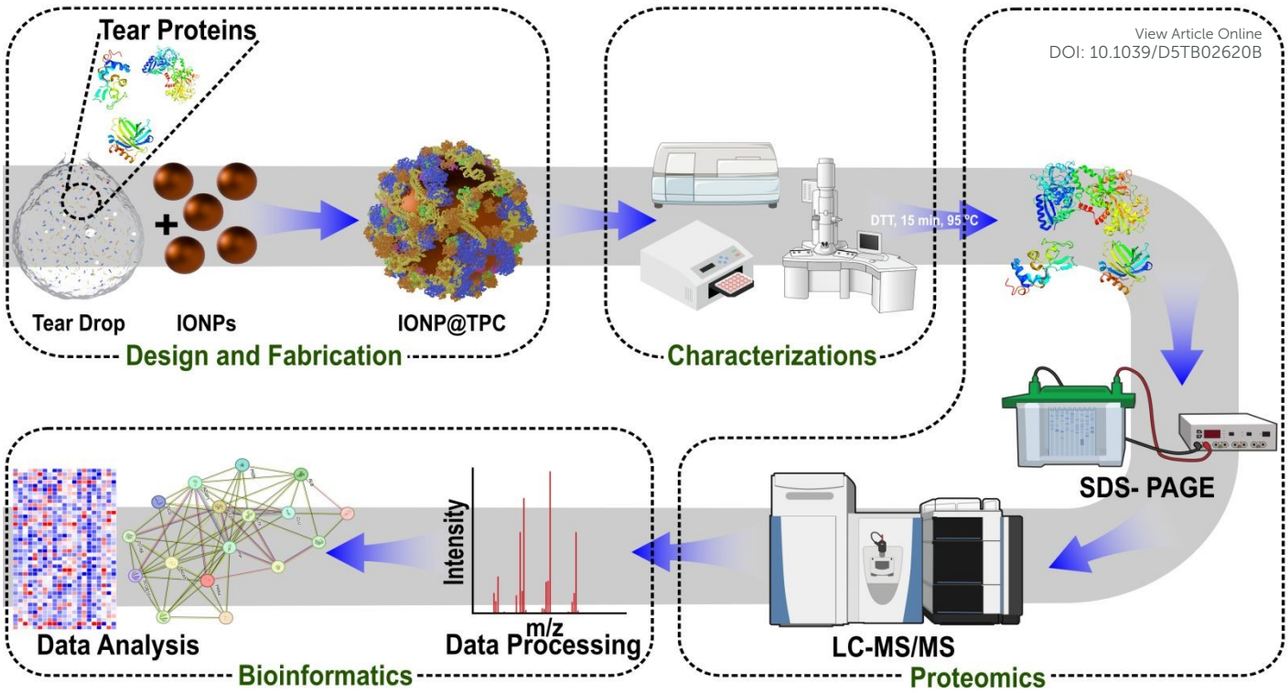

Fig. 1. Stepwise experimental workflow for the design, characterization, and proteomic profiling of the IONP@TPC. IONPs were incubated with human tear extract to form IONP@TPC. The resulting IONP@TPC complex were characterized using physicochemical tools including DLS, zeta potential, and electron microscopy. IONP@TPC samples were treated with DTT for 15 min at 95 °C to extract the particle bound TPC and analyzed using LC-MS/MS-based proteomics. The acquired mass spectra were processed and interpreted using bioinformatics tools to identify and quantify the corona proteins, followed by network-based data analysis.

Figure 2

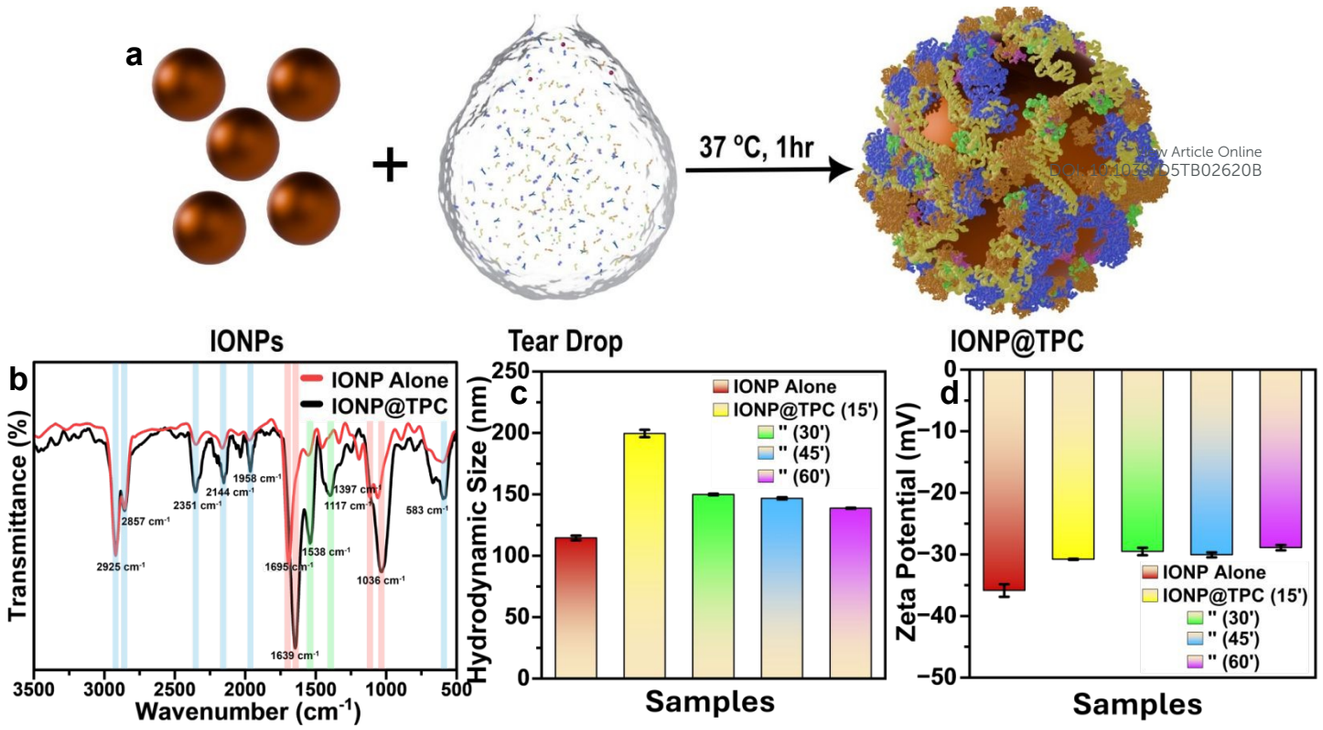

Fig. 2. Schematic of IONP and TPC interactions. Alterations in the hydrodynamic diameter, surface charge and active functional groups of the TPC incubated IONPs. (a) Schematic of the interaction of IONPs with human tear extract forming the IONP@TPC to assess the stability, physicochemical properties. Comparative alterations in the Fourier Transform Infrared spectroscopy (b) hydrodynamic diameter (c) and zeta potentials (d) of the IONP and IONP@TPC samples.

Figure 3

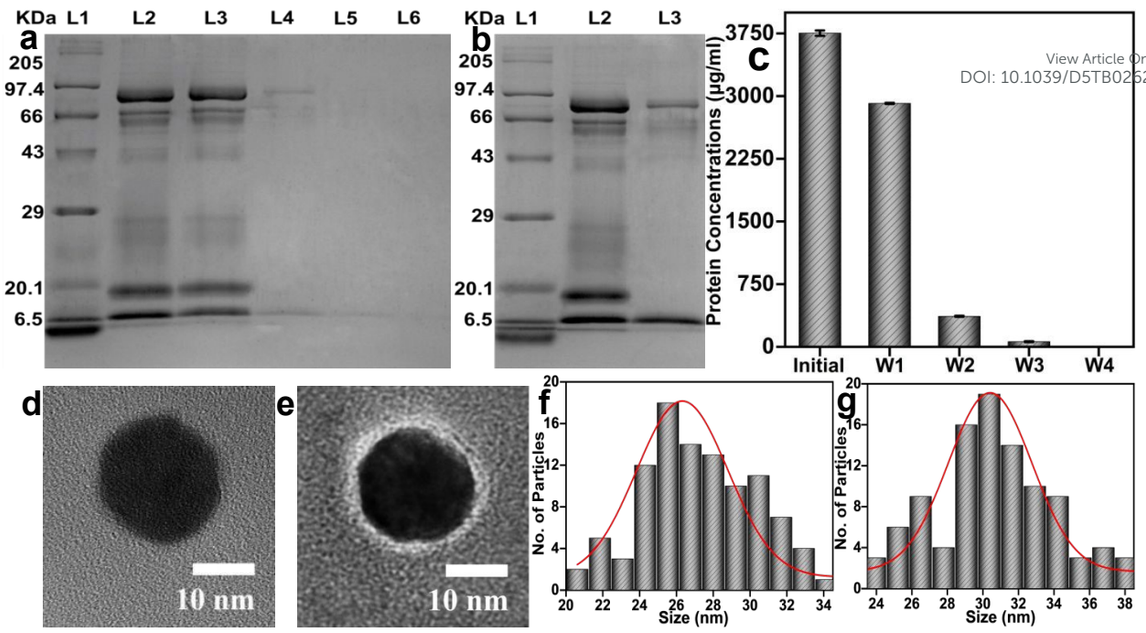

Fig. 3. Evaluation of bound proteins and the morphological alterations upon the interaction of IONPs with human tear extract. (a) Coomassie stained SDS−PAGE gel of the loosely associated tear proteins being washed off during every step of their washing and (Lanes 1: protein ladder, 2: control tear proteins, 3: unbound proteins from first wash, 4: unbound proteins from second wash, 5: unbound protein from third wash, 6 unbound protein from fourth wash:). (b) IONP-bound tear corona proteins extracted using DTT at 95 °C (Lanes 1: protein ladder, 2: control tear proteins, 3: tear protein corona extracted from IONPs. (c) Bradford method of protein quantification during different steps of IONP@TPC purification. (e) TEM images of IONP@TPC, upon negative staining with a layer of proteins adsorbed on the surface of the IONPs unlike IONPs alone controls with no such obvious layer (d). Histogram analysis by counting at least 100 number of nanoparticles showed a small difference in their core diameters which changed from ~27±2 nm (f) to ~31±3 nm (g).

Figure 4

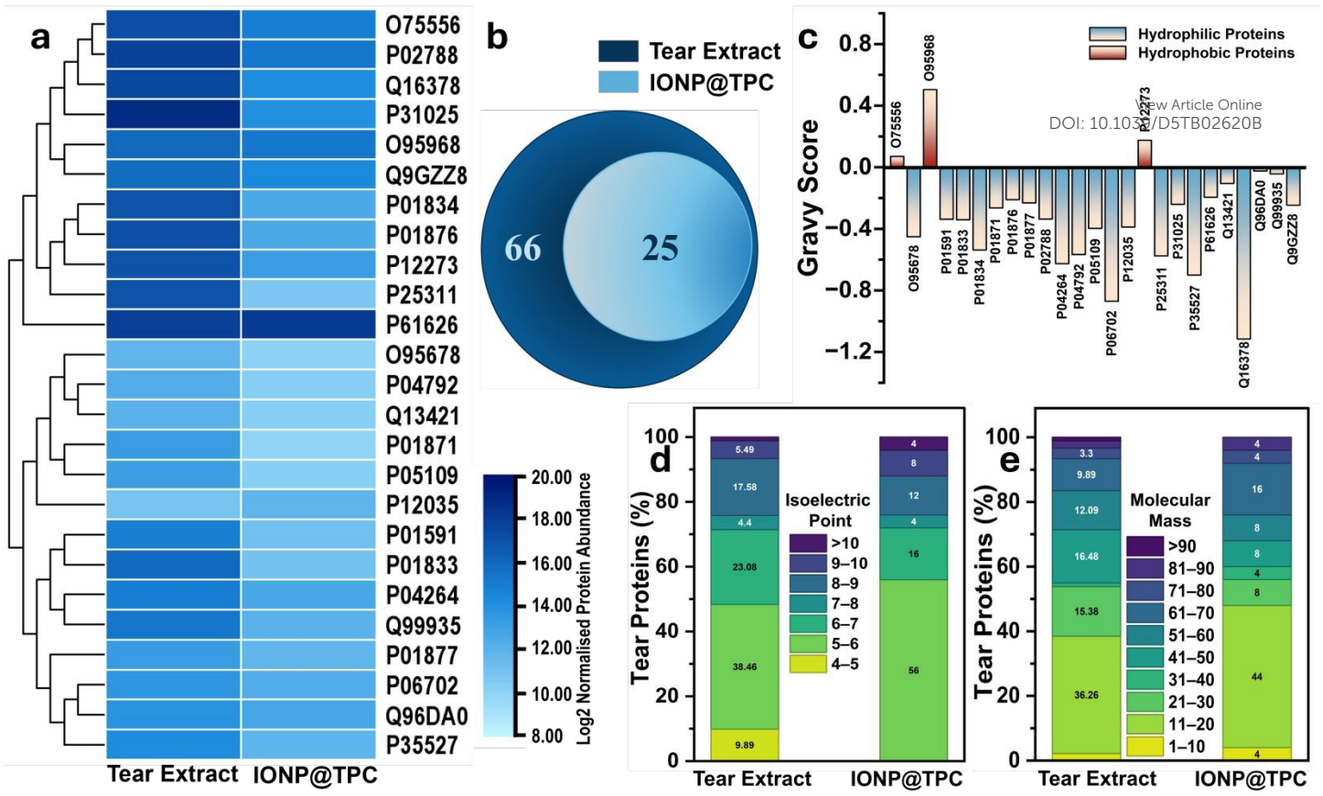

Fig. 4. Proteomic characterization of tear extract proteins and upon adsorption onto iron oxide nanoparticles (IONP@TPC). (a) Heatmap showing clustering of proteins based on their log_2-transformed normalized abundance values of proteins associated with IONP@TPC and their corresponding abundance values in tear extract. (b) Venn diagram illustrating the distribution of proteins between tear extract (66 unbound proteins out of 91 total proteins found) (dark blue) and IONP@TPC that is associated with 25 proteins (light blue) (c) GRAVY (Grand Average of Hydropathy) score analysis reveals that IONP-bound proteins are generally more hydrophilic (blue), except three proteins that were hydrophobic (red). (d) Bar plots depicting molecular weight (MW; left) and isoelectric point (pI; right) distributions of proteins in both groups

Figure 5

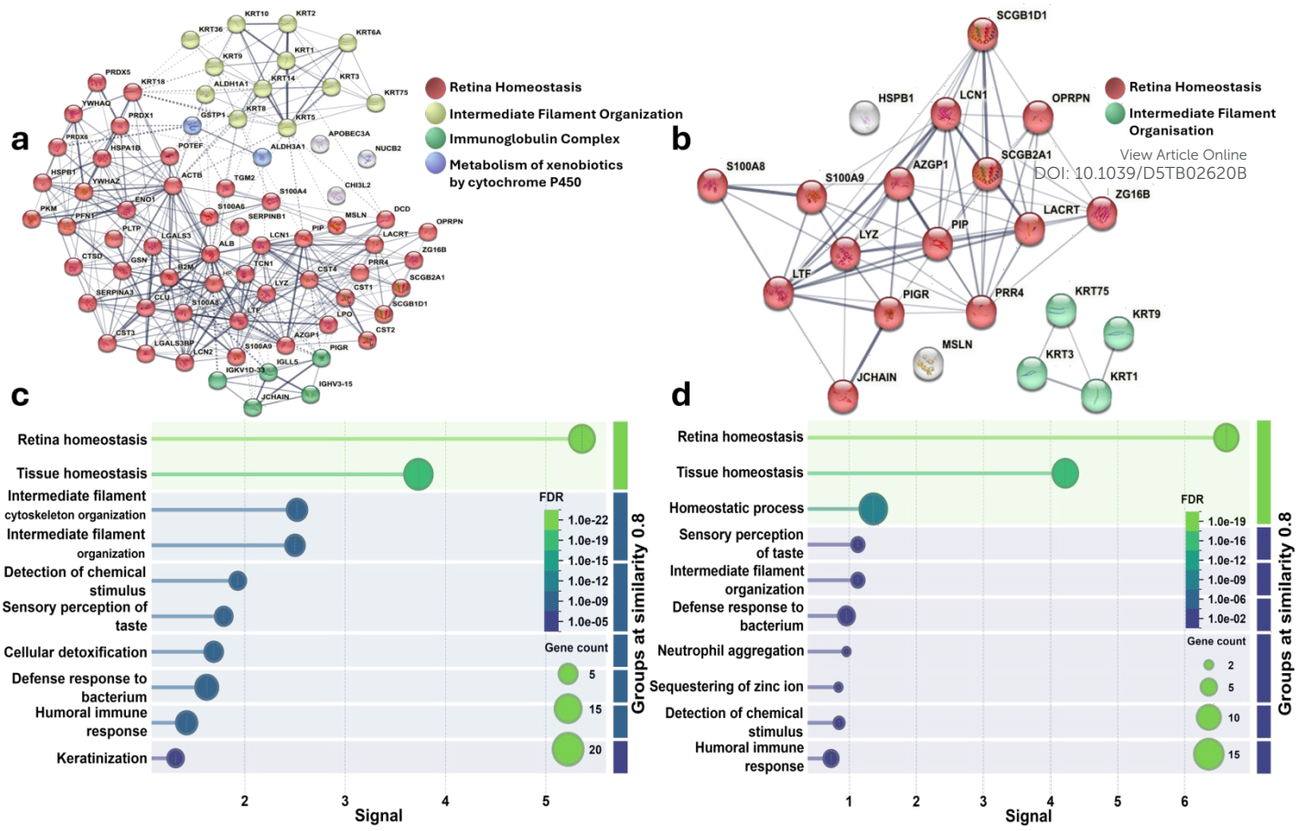

Fig. 5. Interaction network analysis and functional annotation of human tear extract and IONP@TPC associated proteins. (a) STRING protein–protein interaction networks of human tear extract and IONP@TPC-associated proteins. Network visualization of protein–protein associations generated using the STRING database for (a) tear extract and (b) IONP@TPC. Nodes represent individual proteins, and edges indicate functional associations. Distinct clusters corresponding to functionally related protein groups, including structural proteins, immune-related proteins, and secretory components, are observed. Clustering of the network was performed using the Markov Cluster Algorithm (MCL) to identify functionally related groups. (b) Gene Ontology (Biological Process) analysis of proteins of human tear extract and IONP@TPC-associated proteins. Lollipop plot representing the top functional categories identified for (c) human tear extract and (d) IONP@TPC. The x-axis indicates the strength of each functional category, while the y-axis lists the corresponding biological processes. Dot size corresponds to the number of proteins associated with each category (gene count), and colour intensity represents the false discovery rate (FDR), with darker colours indicating higher statistical significance.

Table 1. Alteration in the physicochemical properties of IONPs after protein adsorption when incubated with human tear extract. Abbreviations: dHD: hydrodynamic diameter: nanometer, ζ-potential (mV): zeta potential (electron volts), dTEM: diameter based on transmission electron microscopy (nanometer).

Sample	Colour	dHD (nm)	ζ-potential (mV)	dTEM (nm)	Stability
IONPs	Brown	~115 ± 3.3	-36 ± 1.7	~27±2	Stable
IONP@TPC	Brown	~139 ± 0.7	-29 ± 1	~31±3	Stable

View Article Online
DOI: 10.1039/D5TB02620B

Table 2. Identified tear proteins associated with IONPs with their Uniprot ID, Normalised abundance, Gravy Score, molecular weight and isoelectric point. Abbreviations: MW [kDa]: Molecular weight in kilodaltons, PI: isoelectric point.

UniProt ID	Protein	Normalised Abundance	GRAVY Score	Molecular Weight (kDa)	Isoelectric Point
P61626	Lysozyme C	287238.6332	-0.1946	16536.85	9.4
P02788	Lactotransferrin	39939.26365	-0.337	78181.11	8.5
O95968	Secretoglobin family 1D member 1	38875.18138	0.5044	9898.02	9.4
O75556	Mammaglobin-B	30207.01009	0.0705	10883.73	5.5
Q9GZZ8	Extracellular glycoprotein lacritin	21693.38047	-0.2464	14245.9	5.4
Q16378	Proline-rich protein 4	18486.95528	-1.1157	15096.55	6.5
P31025	Lipocalin-1	16907.2646	-0.2409	19249.79	5.4
P12273	Prolactin-inducible protein	9277.14638	0.1753	16572.28	8.3
Q96DA0	Pancreatic adenocarcinoma up-regulated factor	6743.690684	-0.0244	18878.39	5.4
P04264	Keratin, type II cytoskeletal 1	6513.085057	-0.6258	66037.94	8.2
P01876	Immunoglobulin heavy constant alpha 1	6073.215301	-0.2103	42848.01	5.4
P01834	Immunoglobulin kappa constant	6057.516085	-0.5374	11764.9	6.1
P06702	Protein S100-A9	5203.321269	-0.8702	13241.85	5.7
Q99935	Opiorphin prepropeptide	4123.847318	-0.0435	27216.13	10.4
P35527	Keratin, type I cytoskeletal 9	3689.648286	-0.7006	62063.61	5.1
P12035	Keratin, type II cytoskeletal 3	3647.213387	-0.3889	64416.23	6.1
P01877	Immunoglobulin heavy constant alpha 2	3407.840607	-0.2317	42333.45	5.4
P01591	Immunoglobulin J chain	2306.901457	-0.3377	18098.4	5.1
P01833	Polymeric immunoglobulin receptor	2142.155288	-0.3407	83282.6	5.6
P25311	Zinc-alpha-2-glycoprotein	1739.562235	-0.5758	34258.29	5.7
P04792	Heat shock protein beta-1	1291.530738	-0.5668	22782.23	6.0
P05109	Protein S100-A8	1248.502084	-0.3968	10834.38	6.5
Q13421	Mesothelin	1246.137017	-0.1057	68984.84	6.0
O95678	Keratin, type II cytoskeletal 75	1100.199937	-0.4517	59559.68	7.6
P01871	Immunoglobulin heavy constant mu	1018.082064	-0.2646	51922.94	5.8

View Article Online
DOI: 10.1039/D5TB02620B

Conflict of Interest

There is no Conflict of Interest to Declare

Data Availability Statement

Al the data used in the manuscript is generated by us. All the LC-MS/MS data is deposited at zenodo having a DIO number of 10.5281/zenodo.19401485.